THE ASTROPHYSICAL JOURNAL, 403:426–433, 1993 January 20

SUBMILLIMETER OBSERVATIONS OF THE 1991 JULY 11 TOTAL SOLAR ECLIPSE

M. W. EWELL, JR., H. ZIRIN, AND J. B. JENSEN
Big Bear Solar Observatory, California Institute of Technology, Mail Code 264-33, Pasadena, CA 91125
AND
T. S. BASTIAN
National Radio Astronomy Observatory, P.O. Box O, Socorro, NM 87801
Received 1992 April 16; accepted 1992 July 28

ABSTRACT

We present observations of the 1991 July 11 total solar eclipse at 850 μm made with the Caltech Submillimeter Observatory (CSO) on Mauna Kea. We find that the 850 μm limb is 3380 $\pm$ 140 km above the visible limb. We also find that there is a 10% limb brightening in the outer 7″ of the solar disk, and we measure a central brightness temperature of 6400 $\pm$ 700 K. These results require that the upper chromosphere not be in hydrostatic equilibrium, with a higher electron density than is predicted by the standard (VAL) model. We show that the dependence of limb height on wavelength is well fitted by a one-parameter model with an electron density scale height of 1200 km; there is no need to invoke complex spicule geometry to explain the observations.

Subject headings: eclipses — Sun: chromosphere — Sun: radio radiation

1. INTRODUCTION

The 1991 July 11 total solar eclipse provided an unprecedented opportunity to observe the solar chromosphere and corona. The centerline of the eclipse passed only a few thousand meters south of the prime astronomical real estate near the summit of Mauna Kea. The event did not quite live up to the advanced billing. A cloud of volcanic dust from Mount Pinatubo and atypical high cirrus clouds brightened the sky during totality and added to atmospheric absorption. Still, an opportunity to observe an eclipse at 850 μm with an established observatory will not recur for some time.

Our observations were carried out at second and third contacts when we measured the brightness profile of the solar limb. During totality we measured the brightness temperature of the center of the lunar disk. We used the partial phase to perform a beam calibration. We also took the opportunity of having the CSO rigged for solar work to map the entire sun at 850 and 1250 μm; the results of these mappings are reported elsewhere.

The next section of this paper records the details of our observations. Then the data analysis is described. Finally, we compare our results with previous work and discuss the implications of our results for the structure of the solar chromosphere.

2. OBSERVATIONS

2.1. *Equipment*

The Caltech Submillimeter Observatory was not built with solar observations in mind. The optical surfaces are good enough that pointing the dish directly at the Sun risks focusing an unacceptable amount of near infrared and visible light onto the secondary and detector. To avoid this danger, we constructed a telescope cover out of Griffolyn[1] which is a sandwich made of two thin sheets of polypropylene, one white and one black, with a coarsely woven net of nylon fibers in between. The cover is tough enough to withstand the wind loading when deployed as a 10.4 m sail and is both almost transparent at 850 μm and opaque in the near-infrared and visible (Clark et al. 1983). This technique was devised by G. Hurford and employed previously by Horne et al. (1981). The thickness of the Griffolyn is less than 850 μm and the variation in thickness correspondingly smaller; therefore the cover did not degrade the focus of the telescope.

The detector was superconductor-insulator-superconductor (SIS) tunnel junction receiver tuned to 353 GHz. This device has been described in detail by Ellison et al. (1989).

2.2. *Limb Observations*

We wanted to obtain a high-resolution brightness profile of the solar 850 μm limb and also to measure its height above the visible limb. The most conceptually straightforward way to do this is to point the telescope at the solar limb and then differentiate the observed brightness signal as the solar crescent is either covered or uncovered by the moon. In practice, things were not so simple. During a test run in 1991 January, we tried to track the solar limb and recorded the variations in observed brightness. By assuming that the solar limb profile was a step function, we could approximately determine how the telescope tracking varied in time. We then did computer simulations of observations of second and third contacts, with various solar profiles, but using the known motions of the moon and the derived tracking jitter. These simulations indicated that our results would be too sensitive to pointing errors, and a more complicated experimental design was needed.

We decided to drive the telescope back and forth across the crescent, in what we shall refer to as a "wobble." This method is similar to that employed by Lindsey et al. (1983) to observe the 1981 July 31 eclipse from the Kuiper Airborne Observatory, the only difference being that we have a single beam. The telescope was driven in right ascension with a period of 2 s, meaning that the beam crossed the solar crescent once a second. Although the wobble was performed with respect to the imperfect limb tracking, the actual position of the beam can be determined by using the time of maximum observed signal (as described in § 3.1). Given that the speed of the moon was

[1] Griffolyn is a registered trademark of Reef Industries, Inc., P.O. Box 750250, Houston, TX 77275.

$\sim 0''.5\ s^{-1}$ (Bangert, Fiala, & Harris 1989), this in principal gives a limb profile with 0".5 resolution. The properties of the wobble were determined by observing the motion of the star ϵ Peg in the finder scope. This star was chosen because it was at approximately the same zenith angle as the eclipse would be at the time the wobble details were being worked out. The telescope has a tracking loop with a 0.25 s time constant, so we could select eight points to specify the wobble pattern. The two concerns were minimizing transient pointing errors due to telescope momentum, and obtaining a constant speed sweep across the cresent. We found that an approximately sinusoidal set of driving points gave the desired constant sweep through crescent center and also allowed a reasonably gentle turn around at the edge of the wobble. The points were chosen at equally spaced phases beginning $\pi/8$ from the wobble center to prevent transients there. The amplitude of the wobble was also determined from observations of ϵ Peg, and the required antenna commands to achieve both a 30" amplitude and a 70" amplitude were determined. Note that the sweep speed across the crescent is different for the two amplitudes.

The details of the wobbles are given in Table 1 for each contact. The positions are measured in arcseconds of right ascension and declination relative to Sun center. To correct for possible anomalous atmospheric refraction, we located the half-power points of the solar north, south, and west solar limbs, and thus the position of Sun center, early in the partial phase. The east limb was already eclipsed when the Sun cleared the ridge to the east of the CSO. We verified the position of the west limb ~ 10 minutes before second contact. The times in Table 1 are for the commencement of the wobble; at each contact, the wobble was run for ~ 80 s, collecting 4000 data points at a sampling rate of 50.08 Hz. A higher sampling rate would have been desirable, but we were limited by the size of the computer buffer available to store the data. The WWV time signal was monitored at the observatory, and a time stamp was placed at the beginning of each data file, so we know the time of each observation to 1/60th of a second.

2.3. *Beam Calibration*

A one-dimensional beam calibration was performed during the partial phase of the eclipse after totality. The telescope tracking was halted, and the edge formed by the lunar limb was allowed to drift through the beam. The exact times and positions relative to solar disk center are given in Table 2. The measurements were made in the only part of the solar disk (other than the poles) which was free of active regions and plage. In particular, a plage near disk center prevented the use of that area. Each drift scan consisted of 4000 points at a sampling rate of 50.08 Hz. The edge moved through the beam at the sidereal rate minus the speed of the lunar limb, $13''.4\ s^{-1}$, so the far beam wings were measured. The coordinates were entered manually, so the lunar limb is not exactly time centered in any of the scans.

TABLE 1

LIMB OBSERVATIONS

Contact	Time (UT)	RAO[a]	DECO[a]	Amplitude
2.....	17:27:41.8	945".7	−66"	30"
3.....	17:31:32.4	−941"	115.5	70

[a] Offsets are measured from solar disk center.

TABLE 2

BEAM CALIBRATIONS

Time (UT)	RAO[a]	DECO[a]
18:01:37.4.....	−250"	0"
18:04:35.7.....	−330	0
18:06:25.5.....	−380	0
18:08:19.5.....	−430	0

[a] Offsets are measured from solar disk center.

3. DATA ANALYSIS AND RESULTS

3.1. *Beam Profile*

The beam profile of the CSO antenna has been measured at 290 GHz and 65° zenith angle by Serabyn, Phillips, & Masson (1991), using shear interferometry. They found that the beam had a well-defined core with a 25" FWHM and also a broad 80" "plateau." Scaled to 353 GHz, this is a core of 20.6" and a plateau of 66" We tried to fit our drift scan data using a beam given by the sum of two Gaussians of these widths. We found that there was a significant, much wider component that was not measured by Serabyn et al., so we instead fit the beam as a sum of three Gaussians. First the strength and FWHM of the far wing component was fit to the far wing of the drift scan. Then the strength and width of the plateau component was adjusted to obtain the best overall fit. The width of the core was not allowed to vary. The one-dimensional beam profile is given by

$$G(x) = \frac{0.077}{\sqrt{\pi}} \exp\left[-x^2\left(\frac{2\sqrt{\ln 2}}{20.6''}\right)^2\right] + \frac{0.039}{\sqrt{\pi}} \exp\left[-x^2\left(\frac{2\sqrt{\ln 2}}{73''}\right)^2\right] + \frac{0.02}{\sqrt{\pi}} \exp\left[-x^2\left(\frac{2\sqrt{\ln 2}}{440''}\right)^2\right] \text{mV arcsec}^{-1}.$$

The normalization is chosen so that

$$\int_{-\infty}^{\infty} G(x)dx = 3.2 \pm 0.1 \text{ mV}$$

which is the observed signal (after sky subtraction) from the quiet Sun at the location of the calibration scans. One of the scans is plotted along with the fit in Figure 1. Solar structure interferes with the fits on the bright half of the scans, but the dim halves are very clean, because with only the wings of the beam on the Sun, the structures are averaged over. The slight departure of the fit from the observed scan is due to the plateau component not having a Gaussian profile, but allowing for a more complicated functional form would not significantly change our results. The drift scans were very reproducible—essentially the same fit works for all four calibration scans.

3.2. *Limb Profile*

The data taken during second contact is shown in Figure 2*a*, and the third contact data is shown in Figure 2*b*. Several points are immediately apparent. Each peak corresponds to one scan of the beam across the solar crescent. The height of the peak shrinks or grows with the size of the solar crescent. There is a tendency for the peak widths to alternate in a narrow/wide

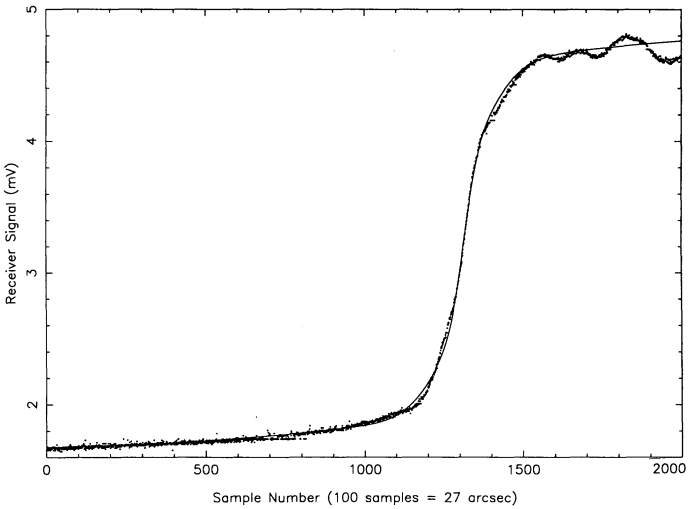

FIG. 1.—A beam calibration drift scan. Only the central 2000 points are shown. The solid line is our three component Gaussian fit.

pattern, especially during the third contact data. This is caused by the Earth's rotation alternately adding to or subtracting from the telescope slew speed. Finally, the wobbling of the beam on and off the moon during totality is readily apparent.

The first step in the data reduction is to subtract out the contributions due to the sky and moon. The expected form of the lunar contribution is easily calculated from the wobble phase and amplitude, the known motion of the lunar limb, and the beam profile. A least-squares fit to the moon-only half of each data set yields values for the moon and sky brightness, and the contributions are then subtracted out. Figure 3 shows the data from both contacts after the subtraction and after smoothing with a robust nonparametric algorithm described by Tukey (1977).

Getting a solar limb profile out of the data is conceptually straightforward, although somewhat complex. The radius of curvature of both the solar and lunar limbs was large compared to the size of the beam core, so to an excellent approximation the exposed solar crescent can be treated as a rectangle. For each contact, the time of each wobble peak was noted, and the Sun was divided into radial bins whose widths are given by the amount of Sun exposed between each successive pair of peaks. (The second contact data was time reversed for this analysis.) One extra bin that ends at the time of the first peak was also used. The peaks are almost evenly spaced, so the bins have approximately equal width. The solar brightness of each bin was computed in turn, beginning with the outermost. For the first bin, the maximum signal occurred when the beam was centered, and the brightness was adjusted to give the observed signal. For the remaining bins, the maximum signal did not necessarily occur when the beam was centred on the exposed crescent, because the crescent did not necessarily have uniform brightness; consequently, an iterative

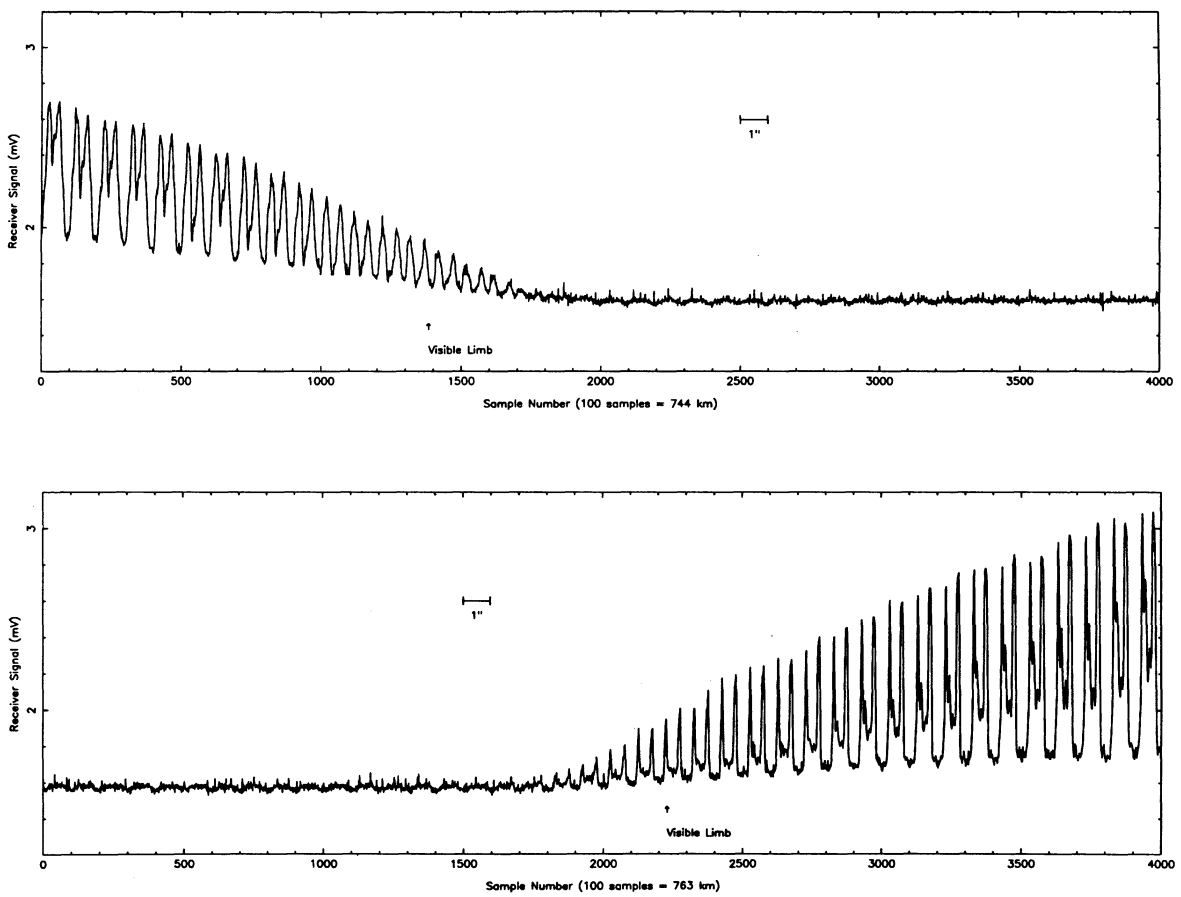

FIG. 2.—The raw data from (*a*) second and (*b*) third contact.

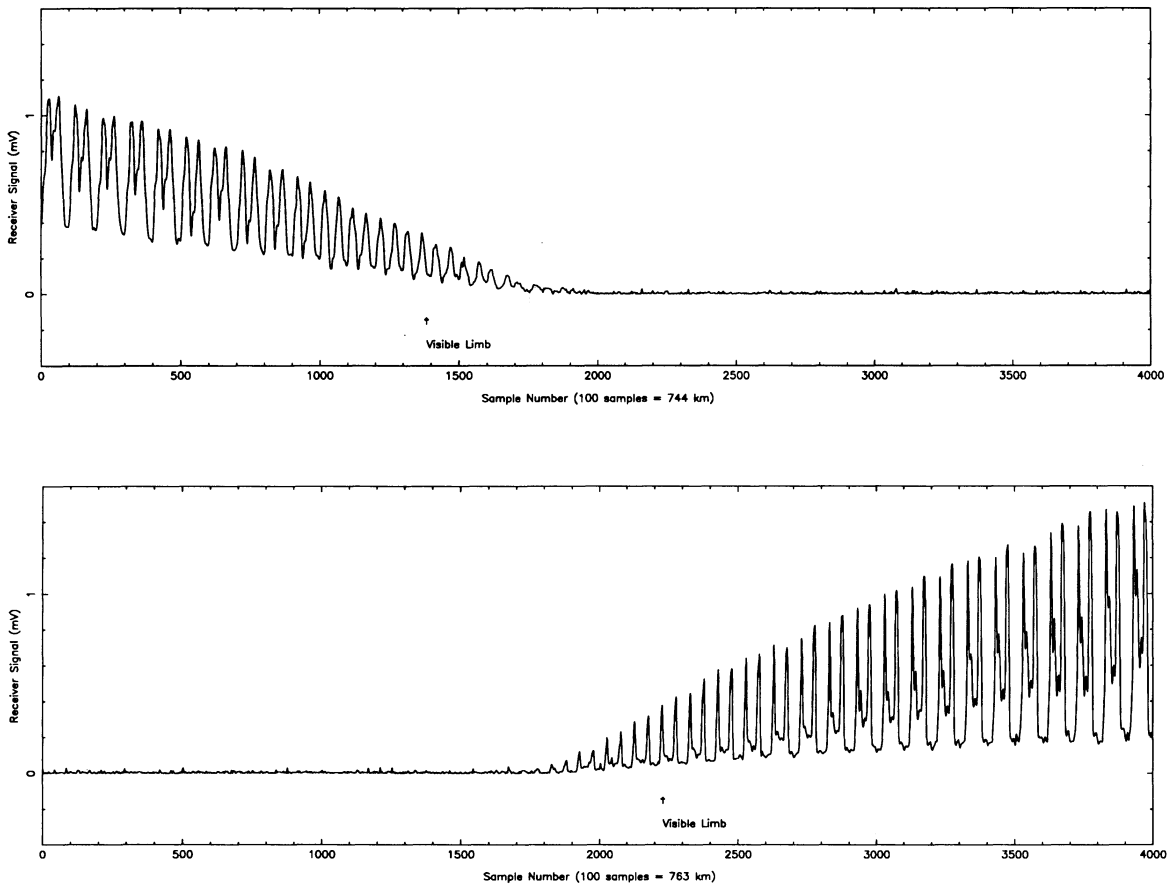

FIG. 3.—The data from (*a*) second and (*b*) third contact after sky subtraction, moon subtraction, the Tukey smoothing.

procedure was required. Each new bin was initially assumed to have the same brightness as the previous bin, the beam position which gave the maximum signal for this brightness was computed, the brightness of the current bin was adjusted to agree with the observed signal, and the process of moving the beam and adjusting the bin brightness was iterated to convergence. Usually only two or three iterations were required. The process was repeated until a brightness had been assigned to each bin, thus determining the limb profile. This procedure performs the beam deconvolution, the pointing correction, and the signal differentiation simultaneously and self-consistently. Note that the beam calibration used was determined from the partial phase drift scans and a measurement of solar disk center brightness, so there is no freedom to adjust the measured temperature scale.

If the procedure described in the previous paragraph is applied to the raw data, a noisy limb profile results. Noise is introduced by the receiver, by changes in the atmosphere, by telescope tracking error, and by the coarseness of the sampling; of these, the atmospheric variations are the most important. The limb profile is basically the derivative of the raw data, so a noisy limb profile is not a surprise. Rather than try to smooth the profile by fitting after the reduction, it is preferable to smooth the data beforehand. We used the data after sky and moon subtraction but before Tukey-smoothing, fitted a simple parabola through the peaks, and then put the fitted brightness values into the above routine. No peak positions were changed by this procedure. The fits to the data from both contacts are shown in Figure 4. It can be seen that the fit is actually very good. No information has been lost by this process. Note that we have excluded the first two points (shown as stars in Fig. 4) from the fit. These points correspond to emission above the limb, and clearly depart from the fit to the remainder of the peaks. The resulting profiles are shown in Figure 5.

The solar limb, defined as the half-intensity point, is easy to identify in the third contact profile. The second contact profile does not have an obvious half-intensity point, so the second contact limb was identified with the peak in the raw data that had the same measured brightness as the third contact limb point. The times at which these data points were taken are given in Table 3, along with the times for the visible contacts with the mean lunar limb, the lunar limb correction, and the speed of the moon. The difference between the submillimeter and visible contact times immediately yields the height of the 850 μm limb. The error bars represent one-half of a wobble period. The extremely close agreement between the two limbs is probably fortuitous. Combining the two measurements gives a limb height of 3380 ± 140 km.

3.3. *Central Temperature*

Our measurement of the brightness temperature of lunar disk center can be used to determine the absolute brightness temperature at the center of the Sun. The receiver signal from the quiet sun was determined during the beam calibration to

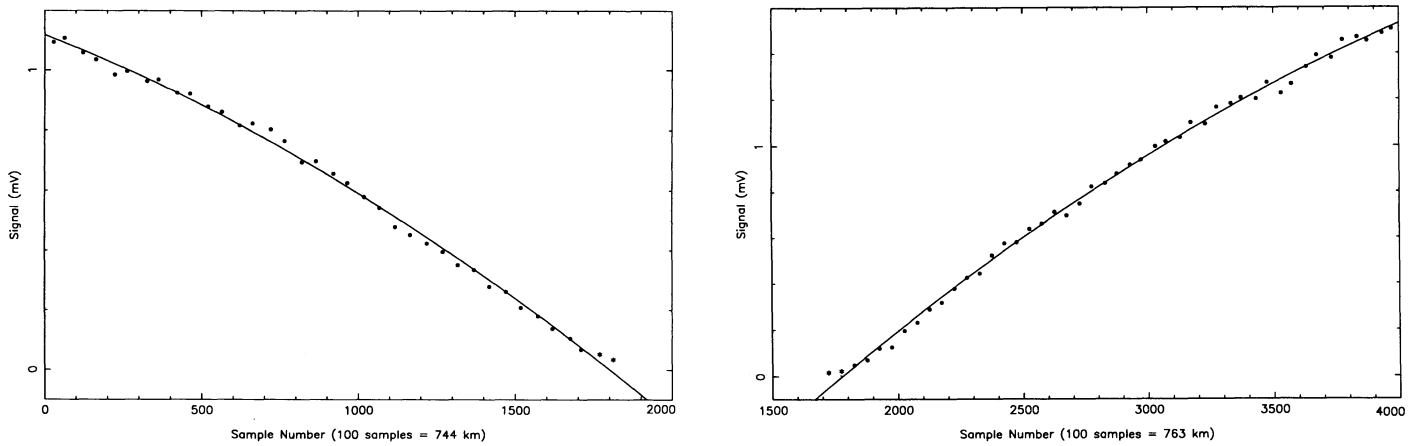

FIG. 4.—The parabolic fits to the (*a*) second contact and (*b*) third contact peaks. The starred data points were not used in the fits, and correspond to emission detected above the limb.

be 3.2 ± 0.1 mV, and the Moon center signal during totality was 0.046 ± 0.002 mV. The surface temperature of the Moon at lunar midnight is 102 ± 3 K (Linsky 1973). Applying the Planck function at 850 μm gives a solar central temperature of 6400 ± 700 K. The primary difficulty with this measurement is that the Sun center and Moon center values were obtained almost 30 minutes apart. The bias introduced by using the solar signal from a somewhat off center point is relatively insignificant. The error bars have been arbitrarily doubled to account for the additional uncertainty due to changes in atmospheric conditions.

4. DISCUSSION

Table 4 compares our measured limb height at 850 μm with published values at several other wavelengths. Note that all the listed heights are referenced to the visible limb and not to the photosphere, which is ~450 km lower. Our measurement is clearly consistent with the values found at shorter wavelengths by Roellig et al., following the established trend of limb height increasing slowly with wavelength. The 3 mm interferometric measurement of this same eclipse by Belkora et al. shows that the trend continues well into the millimeter regime. The values at 1.3 and 2.6 mm are not from eclipse experiments, and their error bars may be understated.

The limb heights predicted by the "standard" model of the solar chromosphere, VAL model C (Vernazza, Avrett, & Loeser 1976, 1981), are also given in Table 4. The 850 μm limb in this model occurs at the height of the transition region, which is why there is no wavelength dependence above this point. There is no doubt that the VAL model is ruled out by the observations. The reason for the discrepancy is clear; the primary observational input to the VAL is from radiation that emanates from below the temperature minimum. The only exception is the Lyα line, which is difficult to interpret. The VAL assumed hydrostatic equilibrium. Earlier works on the chromosphere are filled with references to the deviation from hydrostatic equilibrium, and many explanations were proposed. But with the advent of the VAL, the concept seems to have fallen out of favor. Lindsey et al. (1986) have also shown, based on the observed limb heights between 30 and 200 μm, that the chromosphere cannot be in hydrostatic equilibrium.

At radio wavelengths, the opacity of the chromosphere is due to free-free absorption, a readily understood phenomenon. At chromospheric temperatures, H^- opacity is important only

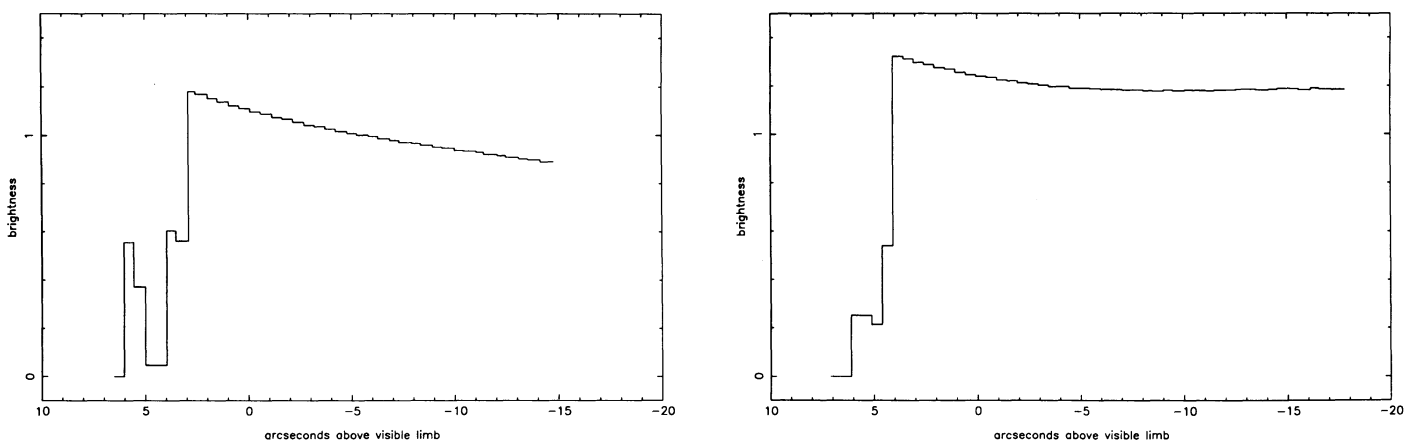

FIG. 5.—The measured solar limb profiles from (*a*) second contact and (*b*) third contact. The peak outside the second contact limb is probably not real, but a result of atmospheric fluctuations.

TABLE 3

MEASURED LIMB HEIGHTS

Contact	Limb Signal Time (UT)	Visible Contact (UT)	Lunar Limb Correction	Speed of Moon (arcsec s^{-1})	Height of Limb (km)
2.....	17:28:18.2	17:28:09.2	+0.2	0.50535	3390 ± 190
3.....	17:32:07.8	17:32:21.2	−4.3	0.51843	3360 ± 190

when the ionization fraction is less than 2×10^{-3} (Athay 1976). For all of the models considered here, optical depth unity in 850 μm occurs much higher in the atmosphere, so we can safely neglect any contribution from H^-. We have constructed a very simple model, the Caltech Irreference Chromospheric Model (or CICM), which fits the observed limb heights using a single adjustable parameter. We use the VAL up to the temperature minimum above which we use an electron density scale height of 1200 km. The scale height is the adjustable parameter. The temperature follows the VAL to the temperature minimum, increases to 6400 K at 1200 km to agree with our disk central temperature measurement and then increases linearly to 7500 K at 5000 km to agree with the temperature measurements of Zirin, Baumert, & Hurford (1991). The limb heights predicted by this model are shown in Table 4. It can be seen that the CICM is in excellent agreement with the observations at all wavelengths. The predictions of the model depend weakly on the assumed temperature at 5000 km, although any value between ~7000 K and 8500 K gives an acceptable fit. The predictions are insensitive to the height at which the temperature rises to 6400 K because the tangential line of sight never penetrates to that depth. Models of the type we propose are not new. Similar densities can be found in the models of van de Hulst (1953) and of Thomas & Athay (1961, chap. 8).

The temperature and density structure of the CICM is presented explicitly in Table 5. The heights are given in kilometers above the photosphere. Note that we include only pro forma total hydrogen densities, because our observations are sensitive only to electron density. The ionization fraction is probably changing rapidly between 1000 and 5000 km, so any conclusion about mass density would require a more detailed calculation. It is clear that the mass density must have a scale height smaller than the 1200 km we find for the electrons.

It is interesting that we can fit the data so well by assuming a smooth atmosphere. Hermans & Lindsey (1986) have shown that the data up to 200 μm can be fitted by "stretching" the VAL, but this method has difficulty fitting the limb heights at longer wavelengths. Lindsey (1987) has shown how, under certain conditions, a rough atmosphere can be statistically treated as a smooth atmosphere, and it is possible that that is the kind of effect we are observing. But any such spicule model must have at least one more free parameter (i.e., the filling factor as a function of height) than we have employed, and the data can be fit without this extra freedom. Also, to get the observed dependence of limb height on wavelength, it is necessary to assume that individual spicules are optically thin. Braun & Lindsey (1987) have proposed a specific model to explain the 100 μm and 200 μm eclipse observations together with the 2.6 m observations of Wannier, Hurford, & Seielstad already referred to in Table 4. They assumed that the number density of spicules with height followed an exponential scaling law, that spicules had a temperature of ~7000 K, and that they were optically thick at 2.6 mm. The requirement for spicules to be optically thick at 2.6 mm is obviated by the results of Belkora et al. (1992), because, as can be seen in Table 4, the Wannier et al. value for the 2.6 mm limb is probably too high. We definitely agree that the chromospheric material we are seeing is at ~7000 K. But the assumptions of an exponential height distribution and that individual spicules be optically thin make the predictions of their model hard to distinguish from ours. Both models have the electron density falling exponentially with height, and their model in addition requires that the electrons be more clumped with height because they have to be concentrated into an exponentially decreasing number of spicules. We prefer the CICM on the basis of simplicity. The geometry of the chromosphere may indeed be complex, but it is not necessary to invoke this complexity to explain the observations.

Additional clues to the structure of the chromosphere come from observations in Hα. In the famous series of limb filter-

TABLE 4

LIMB HEIGHTS AT VARIOUS WAVELENGTHS

Wavelength (μm)	Observed (km)	VAL Limb (m)	CICM Limb (km)	Reference
200	1450 ± 200	900	1550	1
360	2300 ± 200	1400	2300	1
670	3300 ± 200	1700	3100	1
850	3380 ± 140	1800	3400	
1300	6100 ± 700	1800	4300	2
2600	6800 ± 1400	1800	5200	3
3000	5500 ± 400	1800	5400	4

REFERENCES.—(1) Roellig et al. 1991; (2) Horne et al. 1981; (3) Wannier et al. 1983; (4) Belkora et al. 1992.

TABLE 5

CICM

Height (km)	Temperature (K)	N_e (cm^{-3})	N_H (cm^{-3})
500.....	4410	3.01(+11)	2.61(+15)
600.....	4620	2.25(+11)	1.19(+15)
800.....	5220	1.90(+11)	2.50(+14)
1000.....	5820	1.61(+11)	5.25(+13)
1200.....	6410	1.36(+11)	1.10(+13)
1400.....	6540	1.15(+11)	7.37(+12)
1700.....	6620	8.98(+10)	4.05(+12)
2000.....	6700	6.99(+10)	2.22(+12)
2300.....	6780	5.45(+10)	1.22(+12)
2600.....	6860	4.24(+10)	6.69(+11)
2900.....	6940	3.30(+10)	3.67(+11)
3200.....	7020	2.57(+10)	2.01(+11)
3500.....	7100	2.00(+10)	1.11(+11)
3800.....	7180	1.56(+10)	6.07(+10)
4100.....	7260	1.21(+10)	3.33(+10)
4400.....	7340	9.46(+9)	1.83(+10)
4700.....	7420	7.37(+9)	1.00(+10)
5000.....	7500	5.74(+9)	5.50(+9)

grams taken by R. B. Dunn (Lynch, Beckers, & Dunn 1973), the spicule forest is clearly visible in the pictures taken 0.75 and 1 Å away from line center, but at Hα line center, the top edge of the chromosphere appears smooth, and the limb is at a height *above* the spicule forest seen off band. This argues against the electrons being more clumped with height, as postulated by Braun & Lindsey. Recent Hα measurements by Suematsu, Zirin & Wang (1993) show typical spicule lengths of 5000 km with tilts averaging 45°. This argues against the Hα limb representing a line-of-sight merging of the spicule forest and is consistent with the view that spicules are density enhancements in a chromosphere of fairly uniform temperature.

Since the radio opacity depends on N_e^2, one could hope to use Hα to get an independent measure of the density. However, the integrated Hα opacity probably has the same dependence because the fraction of hydrogen in the first excited state depends on density. Calculations of N_2 have been carried out by Poland et al. (1971); these show a fairly wide variation with physical condition, but for our purposes the spicule electron density may be taken as 10^{10}–10^{11} and the population of N_2 as 10^3–10^4. The line absorption in Hα is $l_0 = 10^{-13}$ with a 1 Å line width. This again gives values similar to those obtained from the 850 μm opacity.

In principle, tighter constraints on the temperature structure of the chromosphere can be derived from our observed disk center temperature and limb brightness profile. Unfortunately, the details of the profile are not as trustworthy as the limb height. Our third contact profile (Fig. 5*b*) shows a 10% limb brightening in the outermost 5″. The peak brightness is 1.32 times that at disk center, but the profile is still at 1.18 times disk center 20″ inside the limb. It is not possible to untangle from our data whether the true limb brightening is 30%, or whether the value 20″ inside the limb is the result of a calibration error. Our second contact profile (Fig. 5*a*) has a peak brightness of 1.18 times disk center and falls to 0.89 times disk center at 20″ inside the limb. The uneven structure of the occulation profile, as well as an examination of the raw data, shows that atmospheric fluctuations make this measurement less reliable; we will therefore confine our comments to the third contact measurement. Lindsey et al. (1990) get a limb brightening of 32% at 850 μm using scans with the James Clerk Maxwell 15 m telescope across the solar limb without benefit of an eclipse. This is consistent with the larger of our two possibilities. Roellig et al. (1991) found a 25% limb brightening at 670 μm, but their method is subject to similar calibration difficulties to those that we encountered. The only firm conclusion that can be drawn at the present time is that the 850 μm limb brightening is somewhere between 10% and 35%. The CICM model as described above has a 10% limb brightening compared to disk center. We can accommodate a 30% limb brightening without significantly changing any of the predicted limb heights by reducing the temperature at 1200 km to the VAL value of 5400 K.

The VAL model C predicts a disk central temperature of 5400 K at 850 μm (Vernazza et al. 1981, their Fig. 17). The previous measured values show a large scatter. For example, Eddy et al. (1973) got 6200 K at 700 μm, while Gezari, Joyce, & Simon (1973) got 5900 ± 400 K at 1 mm. A more complete list of previous measurements can be found in Vernazza et al. 1981; Figure 5. More recent work tends to be normalized to the VAL rather than absolutely calibrated. We find 6400 ± 700 K, but the high level of solar activity, as well as the atmospheric conditions, may have affected this value.

Where is the high-temperature component? Clearly there is a small fraction of the chromosphere that is at an enhanced temperature; this is known to coincide with the chromospheric network and mapped out by radio data. However, it is very limited in extent, and appears prominently only in the UV lines, where a large Boltzmann factor greatly magnifies the effects of temperature excess. While the coincidence of these hot regions with the network led to the conjecture that the spicules were the hot component, the present data combined with the eclipse results of others show conclusively that the spicule and general chromospheric temperature is around 6500 K. Since the quiet sun radio spectrum shows 8000 K at longer wavelengths (Zirin et al. 1991), there is a gradual temperature increase taking place at this level.

The picture of a dynamic chromosphere out of hydrostatic equilibrium coming from our data seems consonant with much of what we know about the chromosphere. The powerful reduction in the abundance of low first ionization potential elements in the corona and solar wind, and possibly in the chromosphere, would simply not occur in an atmosphere in hydrostatic equilibrium. Our Hα and K-line images of the chromosphere show a dynamic, constantly moving atmosphere with relatively small variation in brightness temperature. Even the *Skylab* images in He II 304 Å, which might show an enormous exponential variation because of the large value of $h\nu/kT$ at 6000 K, show relatively small brightness variation across the disk. Only optically thin transition region lines show strong variation, which may be attributed to a small number of magnetic hot spots.

5. CONCLUSIONS

We have determined that the 850 μm limb lies 3380 ± 140 km above the visible limb; the upper chromosphere is therefore not in hydrostatic equilibrium. We have measured the 850 μm disk center temperature to be 6400 ± 700 K, and the limb brightening at this wavelength to be between 10% and 35%. This shows that the temperature gradient in the chromosphere is low. We have presented a model chromosphere, the CICM, based on a 1200 km electron density scale height. Our model fits the limb heights observed at all wavelengths between 200 μm and 3 mm. When considered in combination with Hα observations, our results suggest a significant smooth, cool component in the upper chromosphere.

We would like to thank Tom Phillips for letting us point his telescope at the Sun, Gordon Hurford for developing the Griffolyn tent, Michal Peri for help cutting it, Antony Schinckel for his high-altitude acrobatics, and Raoul Taco Machilvich for his computer wizardry. We would also like to thank E. Avrett for several conversations on chromospheric models, and C. Lindsey for his helpful comments.

This work was supported by NSF grant AST-9015139 and AST-9015755, the Zirin Fund, and by a Caltech SURF grant.

REFERENCES

Athay, R. G. 1976, The Solar Chromosphere and Corona: Quiet Sun (Dordrecht: Reidel), 227
Bangert, J. A., Fiala, A. D., & Harris, W. T. 1989, US Naval Obs. Circ., No. 174
Belkora, L., Hurford, G. J., Gary, D. E., & Woody, D. 1992, ApJ, 400, in press
Braun, D., & Lindsey, C. 1987, ApJ, 320, 898
Clark, T. A., Kendall, D. J. W., & Boreiko, R. T. 1983, Infrared Phys, 23, 289
Eddy, J. A., Lee, R. H., MacQueen, R. M., & Mankin, W. G. 1973, BAAS, 5, 271
Ellison, B. N., Schaffer, P. L., Schaal, W., Vail, D., & Miller, R. E. 1989, Int. Infrared Millimeter Waves, 10, 8
Gezari, D. Y., Joyce, R. R., & Simon, M, 1973, A&A, 26, 409
Hermans, L., & Lindsey, C. 1986, ApJ, 310, 907
Horne, K., Hurford, G. J., Zirin, H., & de Graauw, Th. 1981, ApJ, 244, 340
Lindsey, C. 1987, ApJ, 320, 893
Lindsey, C., Becklin, E. E., Jefferies, J. T., Orrall, F. Q., Werner, M. W., & Gately, I. 1983, ApJ, 264, L25
Lindsey, C., Becklin, E. E., Orrall, F. Q., Werner, M. W., Jefferies, J. T., & Gatley, I. 1986, ApJ, 308, 448
Lindsey, C. A., Yee, S., Roellig, T. L., Hills, R., Brock, D., Duncan, W., Watt, G., Webster, A., & Jefferies, J. T. 1990, ApJ, 353, L53
Linsky, J. L. 1973, ApJS, 25, 163
Lynch, D. K., Beckers, J. M., & Dunn, R. B. 1973, Sol. Phys., 30, 63
Poland, A. I., Skumanich, A. S., Athay, R. G., & Tandberg-Hansen, E. T. 1971, Sol. Phys., 18, 391
Roellig, T. L., Becklin, E. E., Jefferies, J. T., Kopp, G. A., Lindsey, C. A., Orral, F. Q., & Werner, M. W. 1991, ApJ, 381, 288
Serabyn, E., Phillips, T. G., & Masson, C. R. 1991, Appl. Opt., 30, 1227
Suematsu, Y., Zirin, H., & Wang, H. 1993, in preparation
Thomas, R. N., & Athay, R. G. 1961, Physics of the Solar Chromosphere (New York: Interscience)
Tukey, J. W. 1977, Exploratory Data Analysis (Reading, MA: Addison-Wesley), 523
van de Hulst, H. C. 1953, The Sun, ed. G. P. Kuiper (Univ. of Chicago Press), Ch. 5
Vernazza, J., Avrett, E. H., & Loeser, R. 1976, ApJS, 30, 1
———. 1981, ApJS, 45, 635
Wannier, P. G., Hurford, G. J., & Seielstad, G. A. 1983, ApJ, 264, 660
Zirin, H., Baumert, B. M., & Hurford, G. J. 1991, ApJ, 370, 779